Journal of Zhejiang University-SCIENCE A (Applied Physics & Engineering)
ISSN 1673-565X (Print); ISSN 1862-1775 (Online)
www.jzus.zju.edu.cn; www.springerlink.com
E-mail: jzus@zju.edu.cn

Thermo-elasto-hydrodynamic analysis of triangular textured mechanical face seals*

Xiao YANG, Xu-dong PENG†‡, Xiang-kai MENG, Jin-bo JIANG, Yu-ming WANG

MOE Engineering Research Center of Process Equipment and Its Remanufacture, Zhejiang University of Technology, Hangzhou 310032, China

†E-mail: xdpeng@126.com

Received Apr. 30, 2019; Revision accepted Sept. 6, 2019; Crosschecked Oct. 17, 2019

Abstract: A 3D thermo-elasto-hydrodynamic (TEHD) model is presented to study the effects of triangular dimples on the load-carrying capacity, leakage and friction of a mechanical seal operated under mixed or full film lubrication conditions. The model is solved by the finite element method (FEM), which takes into account the effects of the Jakobsson-Floberg-Olsson (JFO) cavitation boundary condition, surface roughness, elastic-plastic contact, thermo-elastic deformation, and the temperature-viscosity relation. The numerical results of the TEHD model are quite different from those of the hydrodynamic (HD) and thermo-hydrodynamic (THD) models, especially at high speeds. In order to obtain the optimum shape and distribution of the triangular dimples, a comparative study is conducted to investigate different distributions of equilateral triangles and isosceles right triangles. The results show that a surface textured mechanical seal with isosceles right triangular dimples has the most significant hydrodynamic and pumping effects which, in turn, are beneficial to sealing face opening behavior and leakage limitation. The theoretical results are in good agreement with the experimental ones, and offer new guidance for the future design and development of high-speed mechanical seals for aviation piston pumps.

Key words: Thermo-elasto-hydrodynamic (TEHD); Mechanical seal; Surface texturing; Triangular dimple; Aviation piston pump
https://doi.org/10.1631/jzus.A1900163 **CLC number:** TH117

1 Introduction

A mechanical seal as an important component of aviation piston pumps and thus has a decisive influence on the safety of aircraft. With aircraft development, aviation piston pumps trend towards higher rotation speeds, which creates stringent requirements for the performance of mechanical seals. Surface texturing can be used to enhance the load-carrying capacity and reduce the leakage and friction of mechanical seals. From boundary to full film lubrication conditions, surface texturing is beneficial for reducing friction and wear in many ways (Etsion, 2005). Scholars around the world have made broad scale research on features with different forms and shapes of surface texturing (Etsion, 2004; Gropper et al., 2016). To enhance load-carrying capacity and reduce leakage and friction, surface texturing is widely applied to mechanical seals (Yu et al., 2002; Qiu and Khonsari, 2011). Recently, research has mainly focused on the optimum shape, distribution and structural parameters of textures (Adjemout et al., 2015b; Shen and Khonsari, 2016).

Etsion (Etsion and Burstein, 1996; Etsion et al., 1999), one of the earliest researchers on surface textured mechanical seals, worked on spherical dimples for many years. His research shows that the optimum area ratio of texture for a minimum friction

‡ Corresponding author
* Project supported by the National Natural Science Foundation of China (Nos. U1737202 and 51775505), the National Basic Research Program (973 Program) of China (No. 2014CB046404), the Natural Science Key Foundation of Zhejiang Province (No. LZ15E050002), and the Natural Science Foundation of Zhejiang Province (No. LY17E050018), China
ORCID: Xiao YANG, https://orcid.org/0000-0002-7192-2665; Xu-dong PENG, https://orcid.org/0000-0002-3502-7946

coefficient is about 20%. Bai et al. (2011) presented experimental work on the orientation of elliptical dimples, which shows that the orientation dimple has a significant hydrodynamic effect. Xie et al. (2013) studied the hydrodynamic performances of textured surfaces with different dimples, such as rectangle, triangle, and trapezoid. Theoretical results show that the shapes and orientations of dimples have great influence on load-carrying capacity. Adjemout et al. (2015a) presented a numerical analysis on the shape and distribution of dimples. The results show that a single triangular dimple could not generate a positive load-carrying capacity, while two triangular dimples placed symmetrically with respect to their bases obtained the maximum load-carrying capacity. Compared to square and rectangular shapes, the triangle shape has a strong orientation effect, with a great influence on load-carrying capacity, friction coefficient, and leakage. Similar results can also be seen in other studies (Yu et al., 2010; Zhang et al., 2016), where triangles at different orientations were studied by experimental and theoretical methods.

Although many studies have shown that triangular textures have strong hydrodynamic effects, the texture shapes studied have mostly been equilateral triangles, and there are few studies on right triangles. Moreover, most of the theoretical studies of textured surfaces mentioned above are based on a hydrodynamic (HD) model, without regard to the influence of surface temperature and deformation. There are some studies (Qiu and Khonsari, 2012; Zouzoulas and Papadopoulos, 2017; Meng et al., 2018) of textured or grooved surfaces based on an advanced thermo-hydrodynamic (THD) model. Only a few studies (Adjemout et al., 2018; Yang et al., 2018) are based on the thermo-elasto-hydrodynamic (TEHD) model.

Here, a 3D TEHD model is presented to study the effect of triangular dimples on the performance of mechanical seals. The model considers the effects of the Jakobsson-Floberg-Olsson (JFO) cavitation boundary condition, surface roughness, elastic-plastic contact, thermo-elastic deformation, and temperature-viscosity relation on the lubrication behavior. The study is conducted under the actual operating conditions of mechanical seals for aviation piston pumps. A comparative study of the three models for predicting seal performance, the HD model, THD model, and TEHD model, is performed. The distributions of the right triangular dimples are optimized under given operating conditions. The results provide new guidance for application of the pumping effect and present an optimum distribution of right triangular dimples.

2 Theoretical model

2.1 Texture geometric model

Fig. 1 shows the geometric diagram of a textured mechanical seal that consists of two rings. As shown in Fig. 1, p_i is the atmosphere pressure and p_o is the fluid sealing pressure, r_i and r_o are the inner and outer radii of the sealing surface, respectively. The stator is fixed to the wall, while the rotor is a floating ring and spring loaded. F_{spring} is the spring force, ω is the rotational speed of the rotor. The sealing surfaces of the two rings are rough. The rotor is made of tin bronze and the stator is made of bearing steel (Table 1). The sealing surface of the stator, which has the greater hardness, is textured. Because of the circumferential periodical distribution of the texture, only one periodic area is studied, and a periodic condition is applied on the radial boundaries. The geometric parameters of the textured surface are listed in Table 2.

The balance ratio of the mechanical seal is equal to 1, so that the closing force can be defined as

$$F_{close}=\pi(r_o^2-r_i^2)p_o+F_{spring}. \tag{1}$$

The opening force of the mechanical seal when operating in mixed or full film lubrication conditions can be written as

$$F_{open}=\iint_{\Omega}(p+p_{con})\mathrm{d}x\mathrm{d}y, \tag{2}$$

where Ω is the sealing surface, p is the film pressure, and p_{con} is the contact pressure.

The film thickness between the two sealing surfaces can be given by

$$h=\begin{cases}h_0+\delta, & \text{outside the dimple,}\\ h_0+h_p+\delta, & \text{inside the dimple,}\end{cases} \tag{3}$$

where h is the film thickness, h_0 is the nominal film thickness, h_p is the depth of dimples, and δ is the thermal-elastic deformation of the two rings.

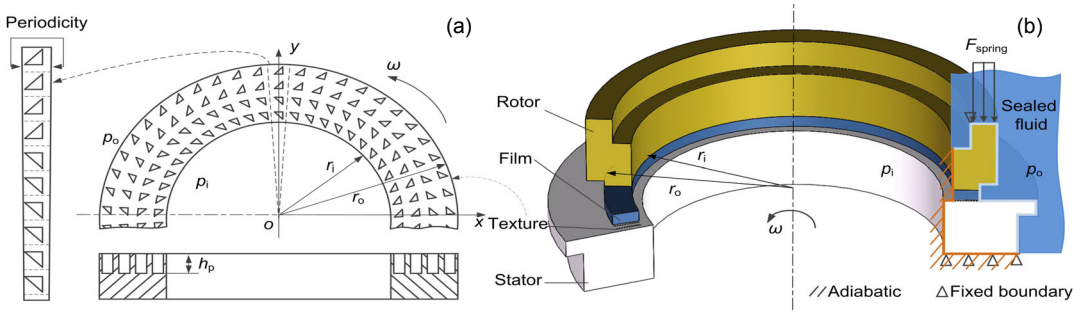

Fig. 1 Geometric structure of the textured mechanical seal
(a) Textured surface; (b) Geometric structure

Table 1 Characteristics of the materials

Parameter	Value	
	Rotor	Stator
Young's modulus, E (GPa)	124	212
Poisson's ratio, v	0.33	0.29
Conductivity, k (W/(m·K))	75	40
Expansion coefficient, α (1/K)	1.72×10^{-5}	1.36×10^{-5}

Table 2 Geometric parameters

Parameter	Value
Inner radius, r_i (mm)	11.90
Outer radius, r_o (mm)	13.95
Depth of dimple, h_p (μm)	5
Periodic number, N	424
Dimple area ratio, S_p	0.2
Surface roughness, σ_r, σ_s (μm)	0.127, 0.192

2.2 Average flow model

Considering the effect of surface roughness on lubrication, the average flow model originally proposed by Patir and Cheng (1978, 1979) and simplified by Wu and Zheng (1989) is employed:

$$\frac{\partial}{\partial x}\left(\phi_x\frac{\rho h^3}{12\mu}\frac{\partial p}{\partial x}\right)+\frac{\partial}{\partial y}\left(\phi_y\frac{\rho h^3}{12\mu}\frac{\partial p}{\partial y}\right)=\frac{U}{2}\phi_c\frac{\partial\rho h}{\partial x}+\frac{V}{2}\phi_c\frac{\partial\rho h}{\partial y}+\frac{U}{2}\sigma\frac{\partial\rho\phi_s}{\partial x}+\frac{V}{2}\sigma\frac{\partial\rho\phi_s}{\partial y}, \tag{4}$$

where μ is the viscosity of the fluid, ρ is the effective density, U and V are the sliding velocities in the x and y directions, respectively, $\sigma=(\sigma_r^2+\sigma_s^2)^{1/2}$ is the standard deviation of the sealing surface roughness, σ_r and σ_s are the sealing surface roughness of the rotor and stator, respectively. ϕ_x and ϕ_y are the pressure flow factors in the x and y directions, respectively (Patir and Cheng, 1978). ϕ_s is the shear flow factor (Patir and Cheng, 1979), and ϕ_c is the contact factor (Wu and Zheng, 1989).

Taking mass conservation into account, the JFO cavitation boundary conditions are introduced to the average Reynolds equation in the numerical simulation. In order to obtain simultaneously the hydrodynamic pressure in both the full film region and the cavitation region, Payvar and Salant (1992) introduced a function Φ, a cavitation index F, and a film fraction θ into the Reynolds equation. They are respectively defined as

$$p-p_c=F\Phi,\quad \theta=\rho/\rho_L=1+(1-F)\Phi, \tag{5}$$

$$\begin{cases}F=1,\ \rho=\rho_L,\ \Phi=p-p_c\geq0, & \text{in the full film region,}\\ F=0,\ p=p_c,\ \Phi=\theta-1<0, & \text{in the cavitation region,}\end{cases} \tag{6}$$

where p_c is the cavitation pressure, and ρ_L is the density of the sealed fluid.

Then Eq. (4) can be re-written as

$$\frac{\partial}{\partial x}\left(\phi_x\frac{h^3}{12\mu}\frac{\partial(F\Phi)}{\partial x}\right)+\frac{\partial}{\partial y}\left(\phi_y\frac{h^3}{12\mu}\frac{\partial(F\Phi)}{\partial y}\right)=\frac{\phi_c}{2}\left(U\frac{\partial[1+(1-F)\Phi]h}{\partial x}+V\frac{\partial[1+(1-F)\Phi]h}{\partial y}\right)+F\frac{\sigma}{2}\left(U\frac{\partial\phi_s}{\partial x}+V\frac{\partial\phi_s}{\partial y}\right), \tag{7}$$

with boundary conditions

$$\begin{aligned} &p(r=r_{\mathrm{i}})=p_{\mathrm{i}},\ \ p(r=r_{\mathrm{o}})=p_{\mathrm{o}},\\ &p(r,-\pi/N)=p(r,\pi/N), \end{aligned} \tag{8}$$

where r is the radius of the sealing surface, and N is the periodic number.

A streamline upwind/Petrov-Galerkin (SUPG) weighted residual method is implemented to the modified Reynolds equation as shown in Eq. (7) and the finite element method (FEM) is used. It adds the diffusion in the flow direction to ensure the stability of the numerical solutions. So the integral weak form of Eq. (7) is expressed as

$$\boldsymbol{A}_{ij}\boldsymbol{\Phi}_j=\boldsymbol{K}_{ij}^{\theta}\boldsymbol{I}_j+\boldsymbol{C}_{ij}\boldsymbol{B}_j, \tag{9}$$

$$\boldsymbol{A}_{ij}=\boldsymbol{K}_{ij}^{p}\boldsymbol{C}_{ij}-\boldsymbol{K}_{ij}^{\theta}(\boldsymbol{I}_{ij}-\boldsymbol{C}_{ij}), \tag{10}$$

$$\begin{cases} \boldsymbol{K}_{ij}^{p}=\iint_{\Omega}\left[\dfrac{h^3}{12\mu}\left(\phi_x\dfrac{\partial \boldsymbol{N}_i}{\partial x}\dfrac{\partial \boldsymbol{N}_j}{\partial x}+\phi_y\dfrac{\partial \boldsymbol{N}_i}{\partial y}\dfrac{\partial \boldsymbol{N}_j}{\partial y}\right)\right]\mathrm{d}x\mathrm{d}y,\\ \boldsymbol{K}_{ij}^{\theta}=\iint_{\Omega}\left[\dfrac{1}{2}\phi_{\mathrm{c}}h\boldsymbol{N}_i\left(U\dfrac{\partial \boldsymbol{N}_j}{\partial x}+V\dfrac{\partial \boldsymbol{N}_j}{\partial y}\right)\right.\\ \left.-\dfrac{\phi_{\mathrm{c}}}{4}h^2\tau^{\mathrm{SUPG}}\left(U\dfrac{\partial \boldsymbol{N}_i}{\partial x}+V\dfrac{\partial \boldsymbol{N}_i}{\partial y}\right)\left(U\dfrac{\partial \boldsymbol{N}_j}{\partial x}+V\dfrac{\partial \boldsymbol{N}_j}{\partial y}\right)\right]\mathrm{d}x\mathrm{d}y,\\ \boldsymbol{B}_j=-\iint_{\Omega}\dfrac{1}{2}\boldsymbol{N}_j\sigma\left(U\dfrac{\partial \phi_{\mathrm{s}}}{\partial x}+V\dfrac{\partial \phi_{\mathrm{s}}}{\partial y}\right)\mathrm{d}x\mathrm{d}y, \end{cases} \tag{11}$$

where $\tau^{\mathrm{SUPG}}=h_{\mathrm{T}}\big/\sqrt{U^2+V^2}$ is the stabilization parameter and h_{T} is the characteristic length of each element in the direction of velocity. $\boldsymbol{N}_i$ and $\boldsymbol{N}_j$ are the shape functions. $\boldsymbol{K}^p$, $\boldsymbol{K}^{\theta}$, and $\boldsymbol{A}$ are the stiffness matrixes, $\boldsymbol{\Phi}_j$ is the vector of the function Φ, $\boldsymbol{B}_j$ is the stiffness vector, $\boldsymbol{I}_{ij}$ and $\boldsymbol{I}_j$ are the identity matrix and vector, respectively, $\boldsymbol{C}_{ij}$ is the diagonal matrix, which has diagonal elements $\boldsymbol{C}_{jj}=\boldsymbol{F}_j$, and $\boldsymbol{F}_j$ is the vector of the cavitation index F. To obtain the hydrodynamic pressure, a detailed description of the iteration procedure can be found in (Meng et al., 2014a, 2014b).

2.3 Elastic-plastic contact model

To consider the contact between two nominally flat rough surfaces, an elastic-plastic contact model proposed by Chang et al. (1987) is employed:

$$p_{\mathrm{con}}=p_{\mathrm{e}}+p_{\mathrm{p}}, \tag{12}$$

$$p_{\mathrm{e}}=\frac{4}{3}\eta E R_{\mathrm{a}}^{1/2}\int_{h-y_{\mathrm{s}}}^{h-y_{\mathrm{s}}+\omega_{\mathrm{c}}}(z-h+y_{\mathrm{s}})^{3/2}\varphi(z)\mathrm{d}z, \tag{13}$$

$$p_{\mathrm{p}}=\eta\pi R_{\mathrm{a}}P_{\mathrm{m}}\int_{h-y_{\mathrm{s}}+\omega_{\mathrm{c}}}^{\infty}[2(z-h+y_{\mathrm{s}})-\omega_{\mathrm{c}}]\varphi(z)\mathrm{d}z, \tag{14}$$

where

$$\omega_{\mathrm{c}}=\left(\frac{\pi P_{\mathrm{m}}}{2E}\right)^2R_{\mathrm{a}},\quad y_{\mathrm{s}}=\frac{0.045944}{\eta R_{\mathrm{a}}},$$

$$\frac{1}{E}=\frac{1-\nu_1^2}{E_1}+\frac{1-\nu_2^2}{E_2},\quad \varphi(z)=\frac{1}{\sigma\sqrt{2\pi}}\mathrm{e}^{-z^2/(2\sigma^2)},$$

where p_{e} is the elastic contact pressure, p_{p} is the plastic contact pressure, P_{m} is the yield stress of the soft material, ω_{c} is the critical interference from the elastic to the elastic-plastic deformation regime, y_{s} is the distance between the mean of the asperity heights and that of the surface heights, E is the equivalent Young's modulus, E_1, E_2 and ν_1, ν_2 are Young's moduli and Poisson's ratios of the rotor and stator, respectively, η is the real density of asperities, R_{a} is the average asperity radius of curvature, and $\varphi(z)$ is the asperity height distribution function, which is assumed to show a Gaussian distribution.

2.4 Heat conduction model

It is assumed that the temperature is constant across the film thickness in the analysis, because the film is very thin. Thus, the temperatures of the two seal rings should be equal on the sealing surface. The two rings of rotor and stator can be regarded as a single model that contains two kinds of materials. The heat conduction equation of the two rings is as follows:

$$\frac{\partial}{\partial x}\left(k\frac{\partial T}{\partial x}\right)+\frac{\partial}{\partial y}\left(k\frac{\partial T}{\partial y}\right)+\frac{\partial}{\partial z}\left(k\frac{\partial T}{\partial z}\right)=0, \tag{15}$$

where T is the temperature, and k is the thermal conductivity of the sealing rings.

Considering that the leakage is low, it can be assumed that the heat flux taken away by leakage is negligible. Thus, the heat flux produced by viscous shear and friction is considered to be entirely transmitted by conduction to the two rings (Luan and Khonsari, 2009). It can be considered as a local heat source on the sealing surface:

$$k\left.\frac{\partial T}{\partial \boldsymbol{n}}\right|_{s_1}-q=0, \tag{16}$$

$$q = q_{\mathrm{v}} + q_{\mathrm{f}} = \frac{\mu r^2 \omega^2}{h} + f_0 p_{\mathrm{con}} r\omega, \tag{17}$$

where $\boldsymbol{n}$ is the normal vector of the boundary, q is the heat flux, q_{v} and q_{f} are the viscous and frictional heat flux respectively, and f_0 is the dry friction coefficient of the sealing surfaces.

Thermal and mechanical boundary conditions can be seen in Fig. 1b. The surfaces of the two rings surrounded by sealed fluid are convective heat transfer boundaries. The surfaces of the two rings exposed to the air are adiabatic boundaries. The bottom surface of the stator is a fixed boundary and also an adiabatic boundary. The bottom surface of the rotor is pushed by a spring, and an axial displacement constraint is applied to its inside diameter. The convection transfer is conducted in the surfaces:

$$k\left.\frac{\partial T}{\partial n}\right|_{s_2} + h_{\mathrm{c}}(T - T_0) = 0, \tag{18}$$

where T_0 is the bulk temperature of the fluid.

The convection coefficient h_{c} is calculated by using Becker (1963)'s empirical formula:

$$h_{\mathrm{c}} = 0.133\frac{k_{\mathrm{L}}}{d}\left(\frac{\rho_{\mathrm{L}}\omega d^2}{2\mu}\right)^{2/3}\left(\frac{\mu C_{\mathrm{p}}}{k_{\mathrm{L}}}\right)^{1/3}, \tag{19}$$

where k_{L} is the thermal conductivity of the fluid, and C_{p} is the isobaric specific heat capacity of the fluid, and d is the outside diameter of the rotor.

The periodic boundary condition of temperature is

$$T(r, -\pi/N, z) = T(r, \pi/N, z). \tag{20}$$

2.5 Thermo-elastic deformation model

In this study, a 3D FEM is used to calculate the thermo-elastic deformation of the two rings. A weak integral form of the thermo-elastic deformation equation is

$$\iiint_V \boldsymbol{B}^{\mathrm{T}}\boldsymbol{D}\boldsymbol{B}\boldsymbol{\delta}\mathrm{d}V - \iiint_V \boldsymbol{B}^{\mathrm{T}}\boldsymbol{D}\boldsymbol{\varepsilon}_{\mathrm{T}}\mathrm{d}V - \iint_S \boldsymbol{N}^{\mathrm{T}}\boldsymbol{P}\mathrm{d}S = 0, \tag{21}$$

and Eq. (21) can also be written as

$$\boldsymbol{K}\boldsymbol{\delta} = \boldsymbol{P}, \tag{22}$$

where

$$\boldsymbol{K} = \iiint_V \boldsymbol{B}^{\mathrm{T}}\boldsymbol{D}\boldsymbol{B}\mathrm{d}V, \quad \boldsymbol{P} = \boldsymbol{P}_{\mathrm{p}} + \boldsymbol{P}_{\mathrm{T}},$$

$$\boldsymbol{P}_{\mathrm{p}} = \iint_S \boldsymbol{N}^{\mathrm{T}}\boldsymbol{P}\mathrm{d}S, \quad \boldsymbol{P}_{\mathrm{T}} = \iiint_V \boldsymbol{B}^{\mathrm{T}}\boldsymbol{D}\boldsymbol{\varepsilon}_{\mathrm{T}}\mathrm{d}V,$$

where the thermal strain vector $\boldsymbol{\varepsilon}_{\mathrm{T}}=\alpha(T-T_0)\{1\ 1\ 1\ 0\ 0\ 0\}$, α is the thermal expansion coefficient, $\boldsymbol{N}$ is the shape function vector, $\boldsymbol{B}$ is the geometric matrix, $\boldsymbol{D}$ is the elasticity matrix, $\boldsymbol{K}$ is the stiffness matrix, $\boldsymbol{P}$ is the nodal load vector, $\boldsymbol{P}_{\mathrm{p}}$ is the load matrix, $\boldsymbol{P}_{\mathrm{T}}$ is the thermal load matrix, and $\boldsymbol{\delta}$ is the displacement vector.

2.6 Temperature-viscosity model

There is a close relationship between fluid viscosity and sealing surface temperature. The temperature-viscosity relationship is described by

$$\mu = a\,\mathrm{e}^{b/(T+c)}, \tag{23}$$

where a, b, c are constants. In this study, an aviation hydraulic oil is used in an aviation piston pump, and it is also used as the sealed fluid. The oil has a high viscosity at a low temperature. At 25 °C the viscosity of the oil is 1.68×10^{-2} Pa·s. The values of a, b, c can be calculated by the methods presented in our previous work (Yang et al., 2018). The upper equation can be expressed as

$$\mu = 3.321\times10^{-4}\,\mathrm{e}^{599.65/(T+127.8)}. \tag{24}$$

2.7 Computation procedures

A 3D TEHD model is solved by using the FEM, and the computational procedure is shown in the flow chart of Fig. 2, which mainly contains three iteration loops. Through the three iteration loops, the closing force is balanced with the opening force, and the film thickness distribution and temperature distribution are all consistent with one another. Once a converged solution is obtained, the sealing performance parameters can be calculated by

$$Q = -\int_{\partial\Omega}\frac{h^3}{12\mu}\left(\phi_x\frac{\partial p}{\partial x}n_x + \phi_y\frac{\partial p}{\partial y}n_y\right)\mathrm{d}l, \tag{25}$$

$$F_{\mathrm{f}} = \frac{1}{r_{\mathrm{m}}}\iint_\Omega \tau r\mathrm{d}x\mathrm{d}y + f_0\times\iint_\Omega p_{\mathrm{con}}\mathrm{d}x\mathrm{d}y, \tag{26}$$

$$\tau=\theta\frac{\mu r\omega}{h}(\phi_{\mathrm{f}}-\phi_{\mathrm{fs}})-\phi_{\mathrm{fp}}\frac{h}{2r}\left(-y\frac{\partial p}{\partial x}+x\frac{\partial p}{\partial y}\right), \quad (27)$$

$$f=F_{\mathrm{f}}/F_{\mathrm{open}}, \quad (28)$$

where Q is the leakage rate, l is the inner circle of the sealing surface, F_{f} is the friction force between the two sealing faces, f is the friction coefficient, r_{m} is the mean radius of the sealing surface, $r_{\mathrm{m}}=(r_{\mathrm{i}}+r_{\mathrm{o}})/2$, and τ is the viscous shear stress. ϕ_{f}, ϕ_{fs}, and ϕ_{fp} are shear stress factors (Patir and Cheng, 1979).

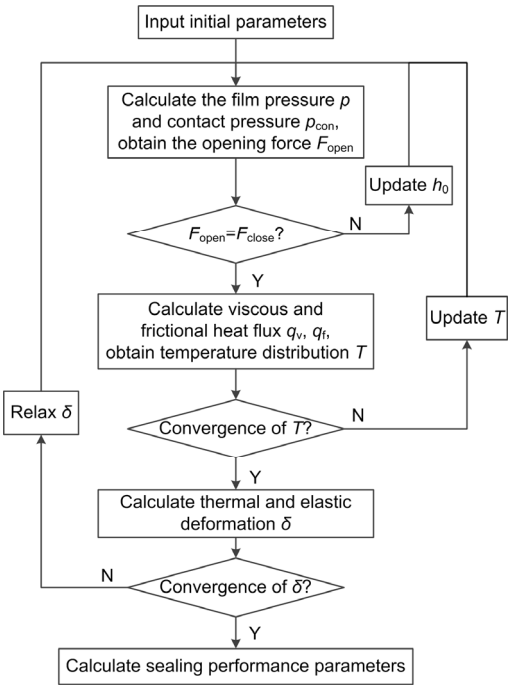

Fig. 2 Calculation flow chart

3 Models and algorithm validation

To verify the 3D TEHD model and the numerical method, comparisons of the simulated results of radial film thickness and radial temperature distributions with the results obtained by Ayadi et al. (2015) were carried out and are shown in Figs. 3 and 4, respectively. In (Ayadi et al., 2015), the stator is rough whereas the rotor is smooth and they are all flat surface, the materials of the rotor and stator are carbon and silicon carbide, respectively, the sealed fluid is water, and the geometrical parameters and operating parameters are given. The results predicted by the present model are in good agreement with those of Ayadi et al. (2015). The maximum error is less than 5%, which indicates the validity of the present model and numerical methods.

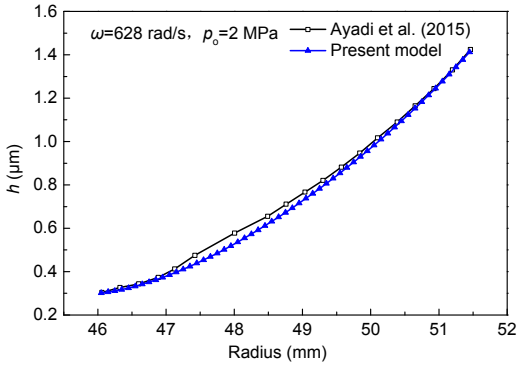

Fig. 3 Comparison of radial film thickness

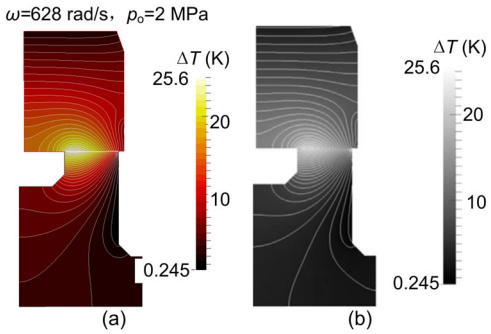

Fig. 4 Comparison of radial temperature distributions
(a) Present model; (b) Ayadi et al. (2015)

4 Results and discussion

The TEHD numerical model is used to investigate the effect of different dimple distributions on sealing performance. The operating parameters are listed in Table 3. The actual working conditions of the mechanical seal in an aviation piston pump can be really simulated with those operating parameters.

4.1 Comparison of the HD, THD, and TEHD models

As shown in Fig. 5, there are two types of triangular textured surfaces which are named 5o-5iE (five triangles at the outer rim and five triangles at the inner rim) and 5o-5i, respectively. The 5o-5iE distribution consists of equilateral triangular dimples,

and the 5o-5i distribution consists of isosceles right triangular dimples. The two triangular textured surfaces are solved by the HD, THD, and TEHD models at different speeds, and the results are shown in Figs. 6 to 10.

Table 3 Operating parameters

Parameter	Value
Atmosphere pressure, p_i (MPa)	0.101
Fluid sealing pressure, p_o (MPa)	0.5
Cavitation pressure, p_c (MPa)	0
Spring pressure, p_{sp} (MPa)	0.3
Rotation speed, n (r/min)	1000–10000
Fluid temperature, T_0 (°C)	25
Dry friction coefficient, f_0	0.1

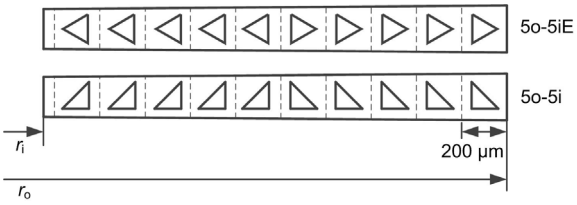

Fig. 5 Triangular textured surfaces

Fig. 6 presents the load-carrying capacity of the two types of triangular textured surfaces. The results show that sealing surfaces with 5o-5iE distribution corresponding to the HD, THD, and TEHD models are in a mixed lubrication condition, except for those corresponding to the HD model when n≥8000 r/min. For the 5o-5iE distribution, the growth rate of load-carrying capacity of the HD model is higher than those of the THD and TEHD models. The reason is that when frictional heat is considered in the THD and TEHD models, the viscosity of the fluid film will decrease with the rotational speed because of the increase of temperature. The lubrication features of the surfaces with 5o-5i distribution controlled by the HD, THD and TEHD models are all in full film lubrication condition when n≥3000 r/min. That means the textured surface with unidirectional right triangles can obtain a higher hydrodynamic effect than that of the surface with bidirectional equilateral triangles.

Fig. 7 presents the average radial clearance of the two textured surfaces when n=10000 r/min. It shows that the average radial clearances of the HD and THD models are constant along the radial direction, which means the two sealing surfaces are parallel. However, the average radial clearance of the TEHD model is convergent, because the surface deformation is considered.

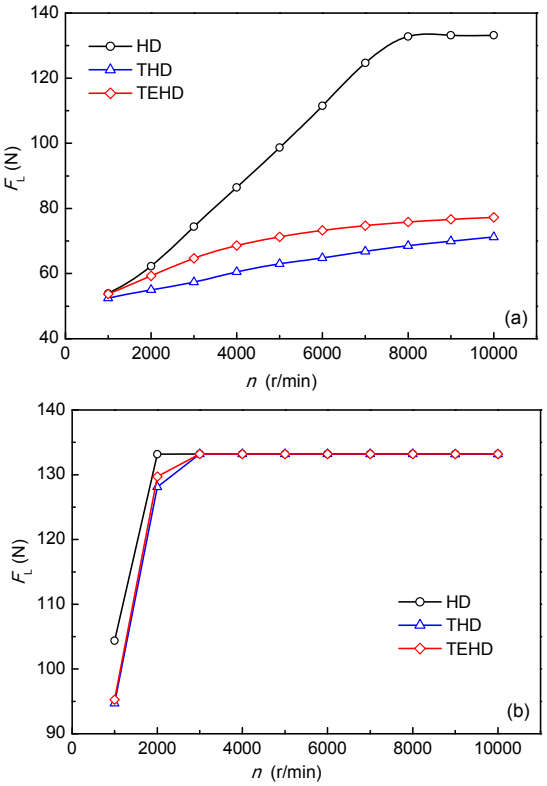

Fig. 6 Comparison of load-carrying capacity
(a) 5o-5iE; (b) 5o-5i

Fig. 8 presents the average film thickness of the two types of triangular textured surfaces. For a textured surface with the 5o-5iE distribution, with the increase of rotational speed, the average film thickness of the HD model increases slowly in the mixed lubrication condition and then increases rapidly in the full film lubrication condition. The average film thickness of the THD model is small and almost constant; it must be very small to provide a suitable contact pressure. The average film thickness of the TEHD model shows a linear increase. Because the surface has a convergent film thickness caused by the deformation, the contact pressure exists near the inner rim. Moreover, the temperature increases with rotational speed, which leads to the increase of deformation, i.e. the convergent angle of film thickness increases, so that the average film thickness increases.

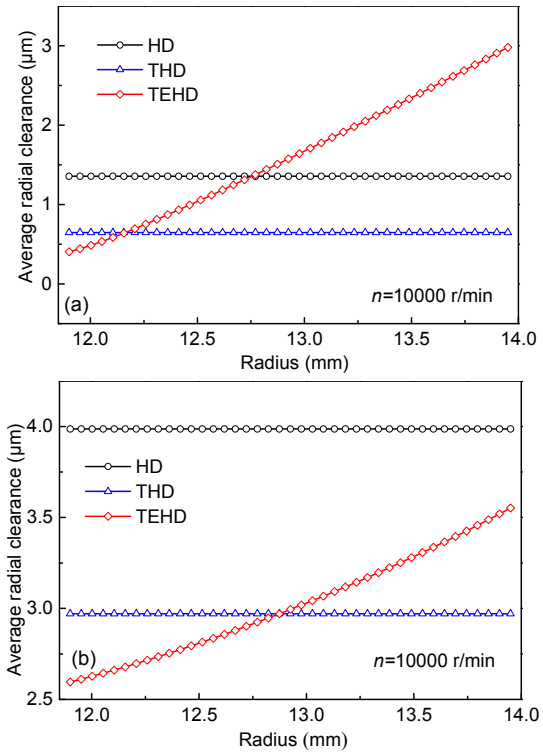

Fig. 7 Comparison of average radial clearances
(a) 5o-5iE; (b) 5o-5i

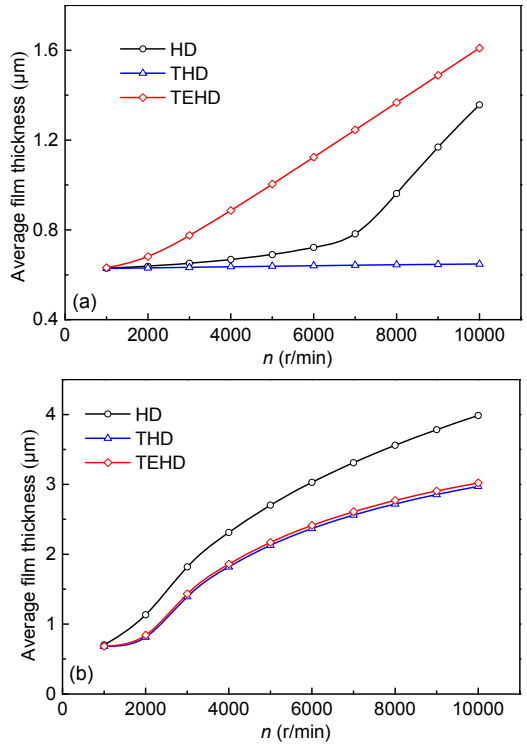

Fig. 8 Comparison of average film thickness
(a) 5o-5iE; (b) 5o-5i

For a textured surface with the 5o-5i distribution, which has a strong hydrodynamic effect and load-carrying capacity, the average film thicknesses of the HD, THD, and TEHD models increase with rotational speed. The average film thickness of the HD model is higher than those of other models, because the temperature is lower and the viscosity of the film is greater, so that the hydrodynamic effect is stronger. The average film thicknesses of the THD and TEHD models are very close, which means the convergent angle of film thickness has little effect on the load-carrying capacity when the surface is in the full film lubrication condition.

Fig. 9 presents the leakage of the two types of triangular textured surfaces. It shows that the leakages of the HD, THD, and TEHD models are different, especially at high speed. For a textured surface with the 5o-5iE distribution, the leakage of the HD model is the lowest when n<7000 r/min, and the largest when n>9000 r/min. Because the temperature is not taken into account, the film has higher viscosity, and the hydrodynamic effect of the textures is stronger, so the surface is in mixed lubrication condition when at low speed, and in full film lubrication condition when at high speed. The leakage of the TEHD model is larger than that of the THD model, for it has a larger average film thickness. It indicates that the leakage mainly depends on the lubrication condition and average film thickness.

Similarly, the leakage of the HD model is the largest for a surface textured with the 5o-5i distribution, which has the largest average film thickness. For the THD and TEHD models, the temperature is taken into account, the film has lower viscosity, and the hydrodynamic effect of the textures is weaker, so the film is thinner. In particular, the average film thicknesses of the THD and TEHD models are very close, but the leakage of the TEHD model is lower than that of the THD model. This can be explained by the difference of film thickness distribution. The deformation is the main influencing factor in the distribution of film thickness. The film thickness of the TEHD model which presents a convergent clearance caused by the deformation of the surface helps to reduce leakage.

Fig. 10 presents the friction coefficient for mechanical seals with two types of textured surfaces. For a textured surface with the 5o-5iE distribution, the

friction coefficient of the TEHD model will increase with the rotational speed, but the friction coefficient of the HD model first increases and then decreases when the surface lubrication conditions change from mixed to full film lubrication. Compared to the HD and THD models, the TEHD model shows the smallest friction coefficient. Moreover, the variation of friction coefficient is very small due to the highest average film thickness and the lower viscosity of the fluid film.

For a textured surface with the 5o-5i distribution, the coefficients of friction controlled by the HD, THD, and TEHD models show the same tendencies with rotational speed. They decrease rapidly, and then increase slowly, because the surfaces are first in mixed lubrication and then in full film lubrication. When the textured surfaces are in mixed lubrication, the load-carrying capacity increases with rotational speed, thus the film thickness increases and the contact friction stresses of the surfaces decrease, which results in a reduction of the friction coefficient. When the lubrication state changes to full film lubrication, the viscosity shearing stress of the oil film increases with rotational speed, which leads to an increase of the friction coefficient. At high speeds, the friction coefficients in the THD model and TEHD model are lower than that in the HD model, because the viscosity of the film is lower when the frictional temperature is considered.

Through comparative analyses of the HD, THD, and TEHD models, it is found that some sealing performance parameters of a mechanical seal with textured surfaces solved by different models are quite different, whether the surfaces are in mixed or full fill lubrication conditions. In particular, the HD and THD models may overestimate the leakage of the surface in the full film lubrication condition or underestimate the leakage of the surface in mixed lubrication condition. Therefore, in order to minimize the friction coefficient while satisfying the requirement of leakage in given conditions, it is necessary to use the TEHD model to study the effects of surface textures.

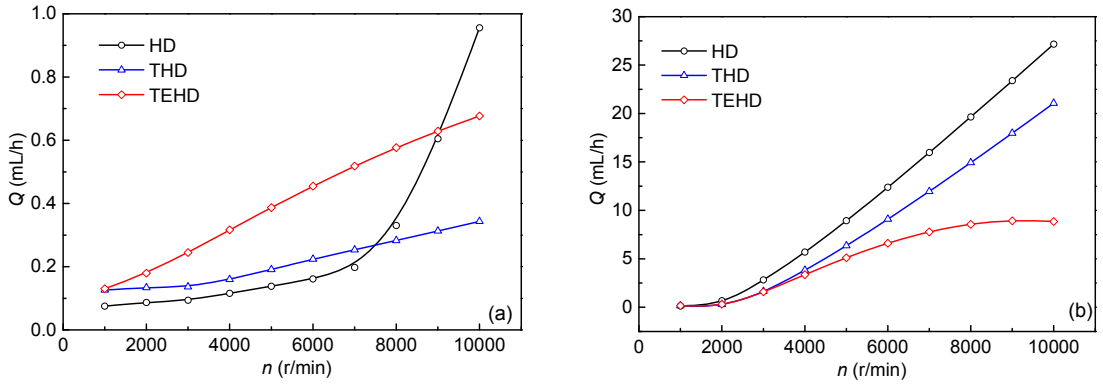

Fig. 9 Comparison of leakage rates: (a) 5o-5iE; (b) 5o-5i

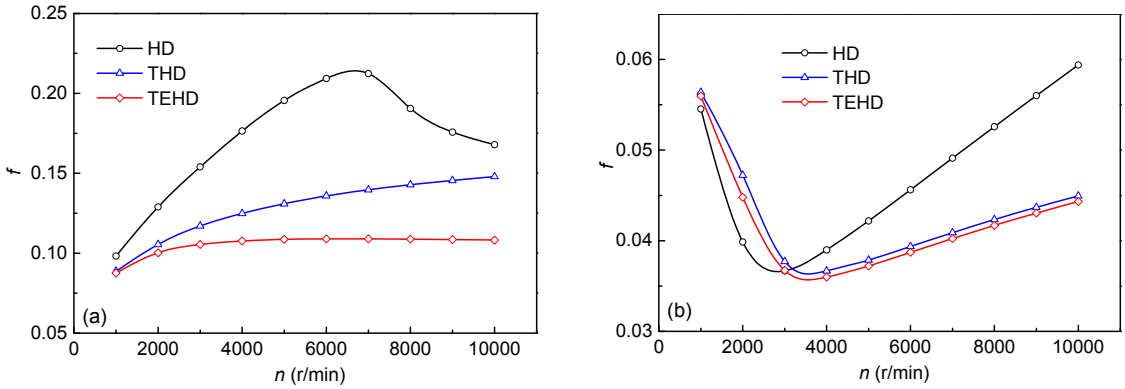

Fig. 10 Comparison of friction coefficients: (a) 5o-5iE; (b) 5o-5i

4.2 TEHD study of the distribution of the triangular dimples

Fig. 11 presents the film pressure, temperature, and deformation of a mechanical seal with a surface texture of 5o-5i distribution when n=10000 r/min. The triangles with apexes placed outwards have downstream pumping and the triangles with apexes placed inwards have upstream pumping. The two opposite pumping effects are combined between sealing faces and a high-pressure zone appears at the middle of the sealing surface. The highest temperature is at the surface near the inside diameter, and the lowest temperature is at the outside diameter. This is due to the high convection coefficient between the outer circumference and the sealed fluid. Because of that uneven temperature distribution, the radial thermal deformation varies with radial position, and the resulted thermal and mechanical deformation leads to a convergent film thickness.

Fig. 12 presents the thermal and mechanical deformation of the textured surface with 5o-5i distribution when n=10000 r/min. It should be noted that the negative values of surface deformation indicate a decrease in the sealing interface of the mechanical seal. The mechanical deformation of the sealing surface leads to a divergent gap between the two sealing faces, while the thermal deformation leads to a convergent gap. The absolute value of the thermal deformation is much larger than that of the mechanical deformation at typical operating conditions of aviation plunger pumps, so the total deformation of the surface causes a convergent gap.

Due to the opposite pumping effect of the symmetrical triangular dimples at the inner and outer rims, the leakage of the textured surface is sensitive to the number of dimples in each of those rims. In order to obtain a lower leakage and friction, several distributions with different numbers of triangular dimples were studied. As shown in Fig. 13, as well as the distributions 5o-5iE and 5o-5i studied above, the distributions 3o-5i, 3o-4i, 2o-3i, 2o-2i, and 1o-2i with isosceles right triangles were also considered.

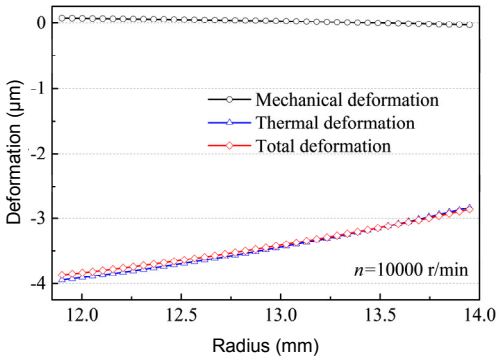

Fig. 12 Thermal and mechanical deformation of the surface with the 5o-5i distribution

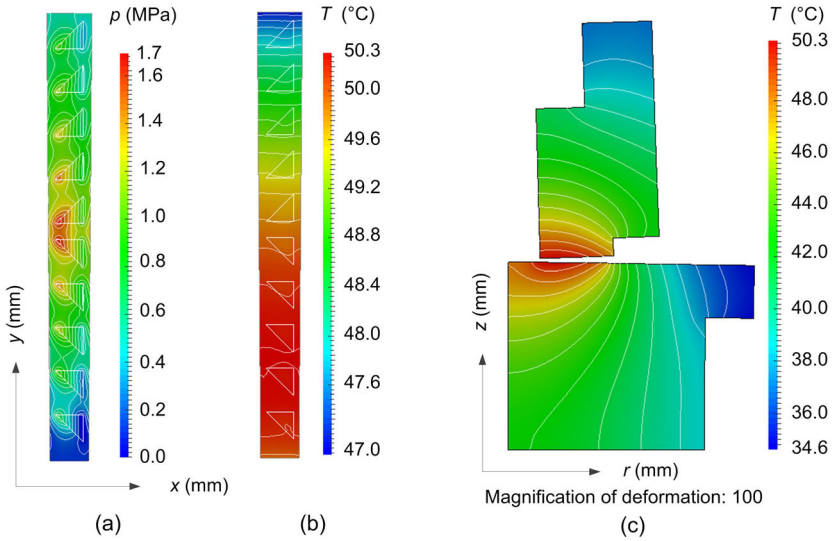

Fig. 11 Film pressure, temperature, and deformation of the mechanical seal (n=10000 r/min)
(a) Fluid pressure; (b) Face temperature; (c) Radial temperature and deformation

Fig. 14 shows the fluid film pressure distributions across the sealing surfaces with different triangular dimple distributions when n=10000 r/min. It can be seen that the pressure distribution of the surface textured with the 5o-5i distribution is higher than that for the 5o-5iE distribution, because the right triangle is more conducive to pressure concentration and the prevention of cavitation. Symmetrical distributions of right triangular dimples, such as 3o-5i, 3o-4i, 2o-3i, and 2o-2i, also produce a high opening force to separate the two sealing surfaces. It means a high hydrodynamic pressure can be obtained even if the number of dimples in the middle region is reduced. The reason is that the upstream pumping and downstream pumping effects of the inner and outer textures can form a high pressure loop in the middle, non-textured, region.

Figs. 15–17 show the face temperature and film thickness distributions and their average value across the sealing surfaces with different triangular dimple distributions when n=10000 r/min. Although the fluid pressure varies at every point of the textured surface, the film thickness seems approximately uniform along the circumference. Because the temperature is relatively uniform along the circumference, and the thermal deformation is much larger than the mechanical deformation, so the total deformation is approximately uniform. It also means that a 2D

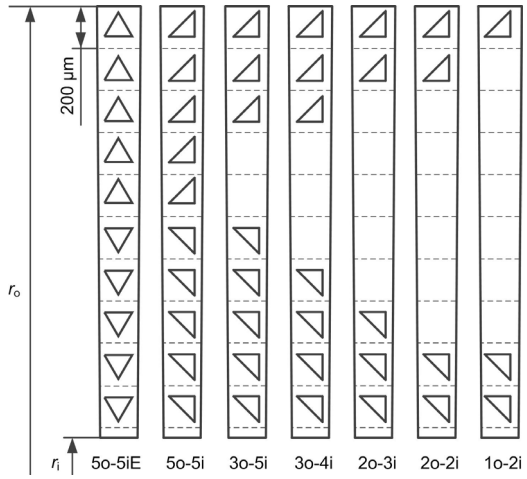

Fig. 13 Different distributions of triangular textured surfaces

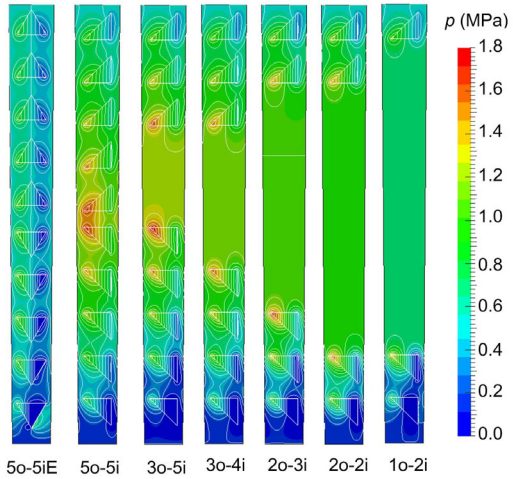

Fig. 14 Fluid pressure of textured surfaces with different distributions (n=10000 r/min)

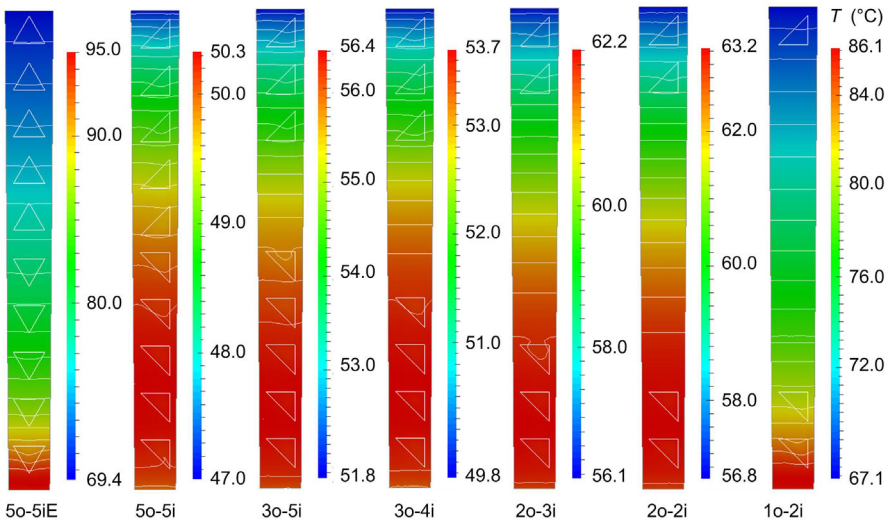

Fig. 15 Face temperature of textured surfaces with different distributions (n=10000 r/min)

axisymmetric model can be used to replace the 3D model to shorten the time required for calculating the deformation of the textured surfaces under a lower sealing pressure.

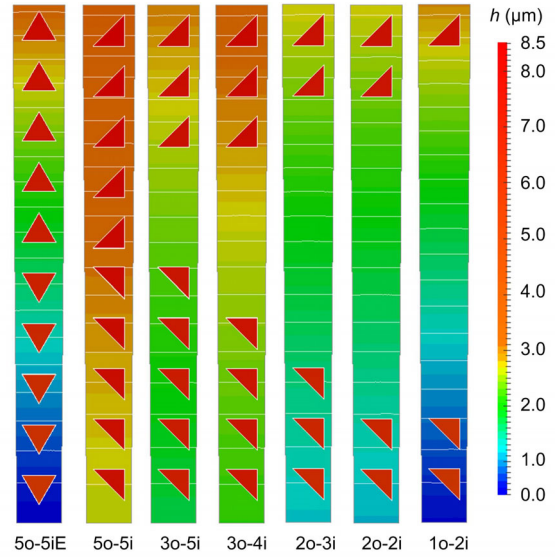

Fig. 16 Film thickness of textured surfaces with different distributions (n=10 000 r/min)

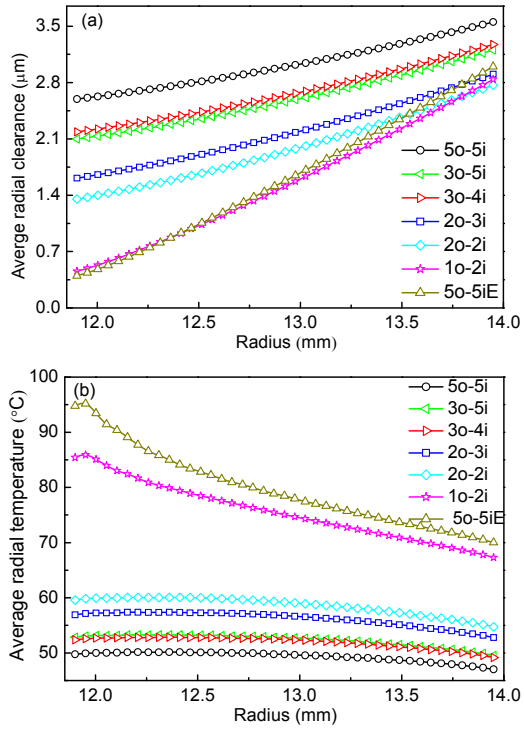

Fig. 17 Average radial clearance (a) and temperature (b) of the textured surface with different distributions (n= 10 000 r/min)

There is a large temperature difference between the inside and outside diameters of the sealing surface textured with distributions of both 5o-5iE and 1o-2i, because a lower fluid film pressure generated by the dimples, which cannot separate the surfaces completely, results in partial contact of the rough surfaces. A quantity of frictional heat is generated in the contact area, resulting in a high surface temperature and a large temperature difference across the sealing surface. Therefore, a large film thickness convergent angle is created by thermal deformation. The surface temperatures of the sealing surfaces textured with the distribution of 2o-2i, 2o-3i, 3o-5i, 3o-4i, and 5o-5i decrease in turn and, in contrast, the film thicknesses of these distributions increase in turn. The reason is that the greater the number of dimples, the greater the pumping effect and, the more balanced the pumping and the reverse pumping effects, the higher the hydrodynamic pressure. In particular, the film thickness of the sealing surfaces textured with the 3o-5i distribution is less than that for the 3o-4i distribution. Because the 3o-5i distribution has stronger upstream pumping effect when the number of dimples on the inside surface is increased, a greater cavitation area and a lower average fluid pressure will occur.

Fig. 18 shows the effects of different distributions on the load-carrying capacity at different speeds. When n≤2000 r/min, the load-carrying capacities of those distributions are lower than that of the closing force, and the sealing surfaces of those distributions are in contact. The load-carrying capacity increases with rotational speed, and the sealing surfaces with the distributions of 5o-5i, 3o-4i, 3o-5i, 2o-3i, and 2o-2i are separated in turn when the load-carrying capacity balances with the closing force. That means the greater the number of dimples located in both the inner and outer sealing surfaces, and the smaller their difference in number, the higher the hydrodynamic pressure that will be produced. In particular, the load-carrying capacity of the 1o-2i distribution increases firstly and then decreases, and the maximum pressure occurs at 5000 r/min. At low speeds the hydrodynamic effects are enhanced, and at high speeds there are two possible effects. One is that, because the number of dimples at the outer rim is twice as that at the inner rim, the upstream pumping effect is much stronger than the downstream pumping effect, and is not conducive to pressure concentration.

The other is that with the increase of rotational speed, the frictional temperature increases, and the convergent angle of film thickness increases, so that the upstream pumping effect of the dimples at the inner rim is enhanced and the downstream pumping effect of the dimples at the outer rim is weakened, further enlarging the strength distinction between the pumping and the reverse pumping effects.

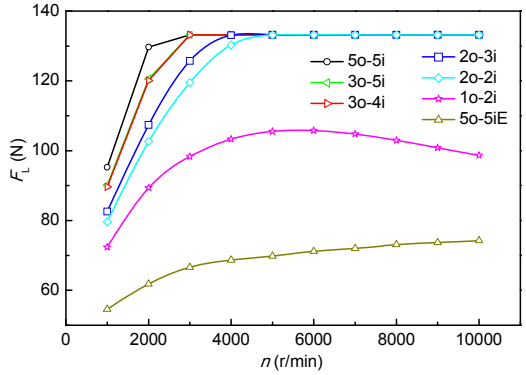

Fig. 18 Effects of different dimple distributions and shapes on load-carrying capacity F_L at different speeds

Fig. 19 shows the effects of different dimple shapes and distributions on the friction coefficient at different speeds. The textured surfaces with the distributions 5o-5iE and 1o-2i have higher friction coefficients, which increase with rotational speed. Because both of those are in a mixed lubrication condition in which the friction coefficient consists of two parts, i.e. contact friction and viscous shear friction, the contact friction decreases with rotational speed, while the viscosity shear friction increases with rotational speed, and the variation rate of the latter friction is higher.

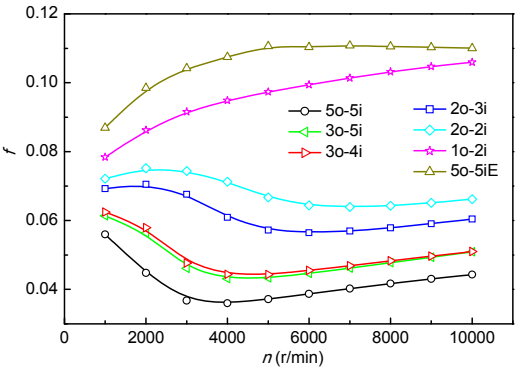

Fig. 19 Effects of different dimple shapes and distributions on friction coefficient at different speeds

The friction coefficients of the distributions 2o-2i, 2o-3i, 3o-4i, 3o-5i, and 5o-5i will decrease firstly and then increase with rotational speed. The curves of the friction coefficients are consistent with the classical Stribeck curve, as the lubrication conditions change from the mixed to the full film lubrication, so that the contact friction decreases rapidly to zero and the viscosity shear friction increases gradually with rotational speed.

Fig. 20 shows the effects of different shapes and distributions on the leakage at different speeds. It should be noted that a positive value of leakage indicates that the fluid is pumped from the mechanical seal to the atmosphere, and the negative value is a pumping flow which indicates that the fluid is pumped back to the high pressure side. The leakage of the distribution 1o-2i is near zero. Sealing surfaces textured with the distributions 5o-5i, 2o-2i, and 5o-5iE have a positive leakage, which means that the upstream pumping effect is smaller than the downstream pumping effect when the number of inner and outer textures is equal. To reduce the leakage, the number of upstream pumping textures should be increased. Thus, the distributions 3o-5i and 2o-3i show a pumping flow, and the 2o-3i distribution has a lower absolute pumping flow, and can be regarded as the optimum distribution. This means that there are fewer textures with the optimum distribution, and their hydrodynamic pressure just transforms the surface lubrication conditions from the mixed to the full film lubrication, in which a lower friction and leakage are obtained.

When textured surfaces with right triangular dimples are completely separated, the upstream pumping effect of the inner triangles increases faster than the downstream pumping effect of the outer triangles as the speed increases. This makes the leakage slow down and the growth of the pumping rate can be accelerated. It means that the increase of rotational speed is more conducive to enhancing the upstream pumping effect of the inner dimples. Particularly, the 3o-4i distribution shows positive leakage when n<7000 r/min, and negative pumping when n>8000 r/min. The reason for this can be seen from the results shown in Fig. 21, which show the pressure distribution and streamlines generated by pressure in

the 3o-4i distribution. With the increase of rotational speed, the enhancement of the hydrodynamic pressure on the inner dimples is greater than that on the outer dimples, which makes the maximum pressure on the inner side increase. When the maximum pressure on the inner side is greater than that on the outer side, the fluid flow mode will change from leakage to pumping.

4.3 Influence of the dimple depth

Fig. 22 shows the average radial clearances of the 2o-3i distribution with different dimple depths when n=10 000 r/min. It shows that the minimum film thickness increases first and then decreases with the increase of dimple depth. When 2 μm≤h_p≤5 μm, the minimum film thickness is larger than 3σ, so that the textured surfaces are in full film lubrication. This means the hydrodynamic effect of the dimples is stronger and the load-carrying capacity is larger when 2 μm≤h_p≤5 μm. The maximum radial clearance occurs when h_p is equal to 4 μm; it is also the optimal dimple depth for the strongest hydrodynamic effect.

4.4 Experimental study

The experimental device is shown in Fig. 23. The seal chamber contains double sets of the same mechanical seal, and the upper one is the test seal. There are seven holes on the back of the stator, which are used to measure the temperature of the sealing surface. The diameter of the holes is 2 mm, and the distance between the holes and the sealing surface is 0.5 mm. The surface of the stator with dimples is

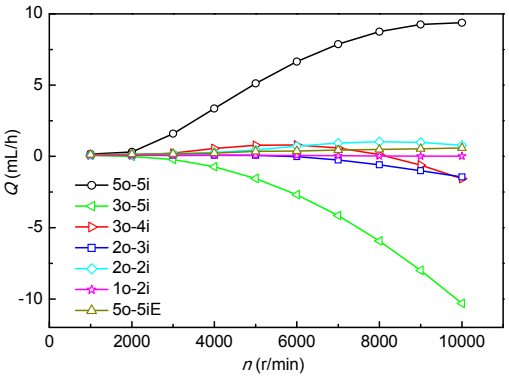

Fig. 20 Effects of different dimple shapes and distributions on leakage at different speeds

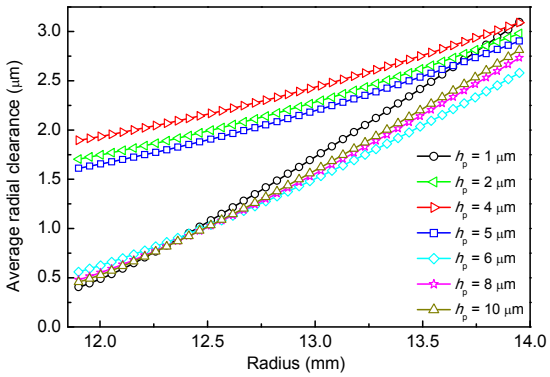

Fig. 22 Average radial clearance of the 2o-3i distribution (n=10 000 r/min)

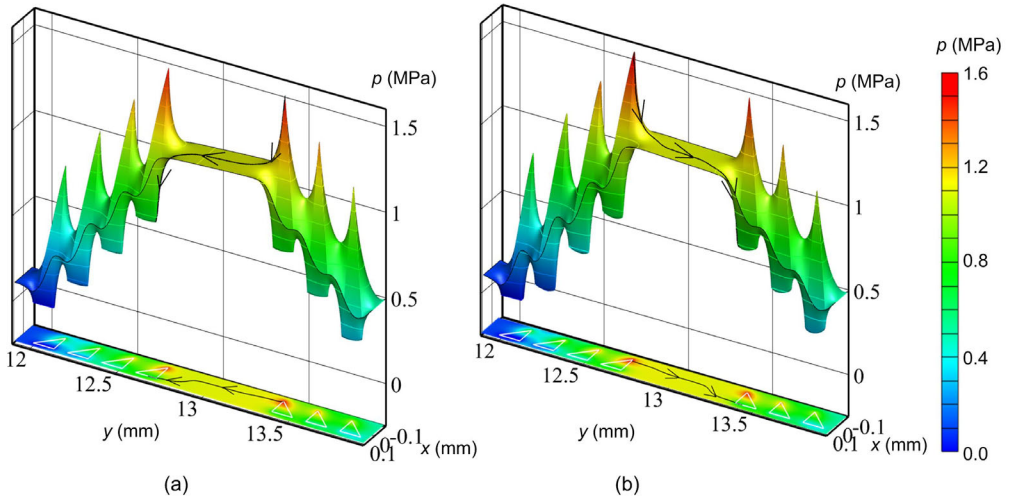

Fig. 21 Pressure distribution and streamlines of the 3o-4i distribution
(a) n=5000 r/min; (b) n=10 000 r/min

shown in Fig. 24, the depth of dimples is about 5 μm, and the dimples are produced by laser surface texturing (LST) technology. The oil in the sealing chamber is supplied by an oil tank, and the pressure of the sealing chamber is kept at 0.5 MPa. Tests were performed at rotation speeds of 1000, 2000, 3000, 4000, 5000, 6000, 7000, 8000, 9000, and 10000 r/min.

Fig. 25 shows the average temperature rise of the sealing surface with the distributions 5o-5i, 2o-3i, and 5o-5iE at different speeds. The temperature of the textured surface increases with the increase of the rotational speed. The temperature rise of the 5o-5i distribution is the lowest and that of the 5o-5iE distribution is the highest. The theoretical and experimental results are thus in good agreement, which shows that the theoretical results are correct.

5 Conclusions

This paper presents a 3D TEHD model to analyze the effects of triangular dimples on the load-carrying capacity, leakage, and friction of a mechanical seal for an aviation piston pump. The

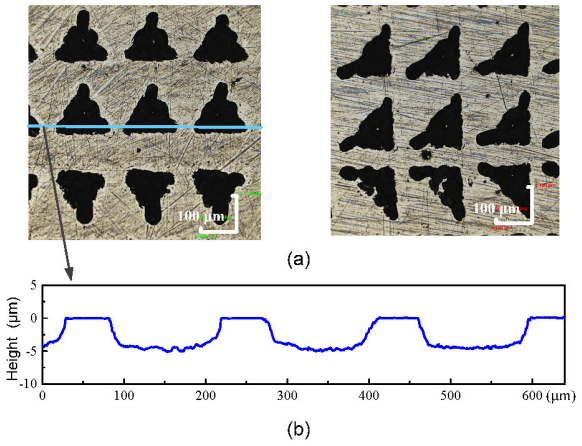

Fig. 24 Surface of stator with dimples
(a) Textured surfaces; (b) Depth of dimples

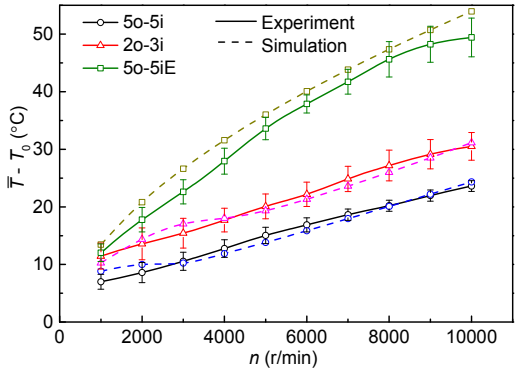

Fig. 25 Average temperature increase of the sealing surface with different distributions

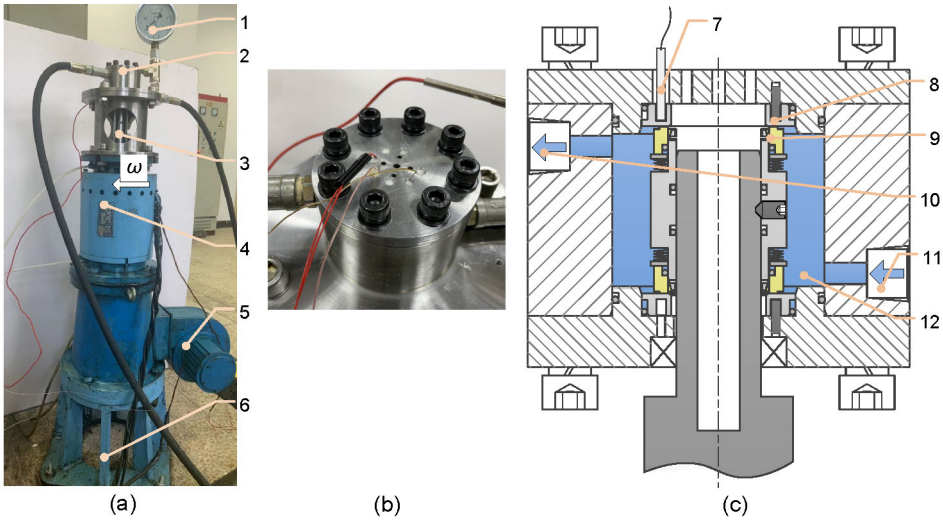

1: pressure gauge; 2: seal chamber; 3: shaft; 4: electric motor; 5: fan; 6: base;
7: thermal resistance; 8: stator; 9: rotor; 10: oil outlet; 11: oil inlet; 12: sealing fluid

Fig. 23 Experimental device of mechanical seals
(a) Experimental device; (b) Seal chamber; (c) Structural diagram of seal chamber

model can simulate the pressure, temperature, and thermo-elastic deformation of the rough-textured surface. A comparative study is conducted in HD, THD, and TEHD models, and the TEHD model is used to optimize the shape and distribution of triangular dimples. An experiment was carried out to verify the correctness of the TEHD model. From the results presented above, the following conclusions can be obtained:

1. The temperature and the deformation in the TEHD model have significant influence on the film thickness, load-carrying capacity, leakage, and friction. The thermal deformation is far greater than the mechanical deformation, resulting in a convergent clearance of sealing surfaces, which enhances the upstream pumping effect of the dimples at the inner rim and weakens the downstream pumping effect of the dimples at the outer rim, leading to a reduction in the leakage.

2. Increasing the number of dimples at the inner rim helps to reduce leakage, but when the number of dimples at the inner rim is much larger than that at the outer rim, the load-carrying capacity will decrease due to the imbalance between the pumping and reverse pumping effects.

3. The hydrodynamic effect of the isosceles right triangular dimple is stronger than that of the equilateral triangular dimple. The 5o-5i distribution of isosceles right triangular dimple has the highest hydrodynamic effect, while when reducing the number of dimples, the distributions 3o-5i, 3o-4i, 2o-3i, and 2o-2i can also produce a higher hydrodynamic pressure to keep the surface well separated when n>4000 r/min, and their friction coefficients decrease firstly and then increase with the increase of rotational speed, due to the change of lubrication conditions from mixed to full film lubrication.

Contributors

Xiao YANG and Xu-dong PENG designed the research. Xiao YANG processed the corresponding data and wrote the first draft of the manuscript. Xu-dong PENG, Xiang-kai MENG, Jin-bo JIANG, and Yu-ming WANG helped to organize the manuscript. Xiao YANG, Xu-dong PENG, Xiang-kai MENG, and Yu-ming WANG revised and edited the final version. Xu-dong PENG reviewed the manuscript and examined the mathematic model, and experimental and simulated results.

Conflict of interest

Xiao YANG, Xu-dong PENG, Xiang-kai MENG, Jin-bo JIANG, and Yu-ming WANG declare that they have no conflict of interest.

References

Adjemout M, Brunetiere N, Bouyer J, 2018. Friction and temperature reduction in a mechanical face seal by a surface texturing: comparison between TEHD simulations and experiments. *Tribology Transactions*, 61(6): 1084-1093. https://doi.org/10.1080/10402004.2018.1478053

Adjemout M, Brunetiere N, Bouyer J, 2015a. Numerical analysis of the texture effect on the hydrodynamic performance of a mechanical seal. *Surface Topography: Metrology and Properties*, 4(1):014002. https://doi.org/10.1088/205-672X/4/1/ 014002

Adjemout M, Brunetiere N, Bouyer J, 2015b. Optimization of mesh density for numerical simulations of hydrodynamic lubrication considering textured surfaces. *Proceedings of the Institution of Mechanical Engineers, Part J: Journal of Engineering Tribology*, 229(9):1132-1144. https://doi:10.1177/1350650115574535

Ayadi K, Brunetiere N, Tournerie B, et al., 2015. Experimental and numerical study of the lubrication regimes of a liquid mechanical seal. *Tribology International*, 92:96-108. https://doi.org/10.1016/j.triboint.2015.05.022

Bai SX, Peng XD, Li JY, et al., 2011. Experimental study on hydrodynamic effect of orientation micro-pored surfaces. *Science China Technological Sciences*, 54(3):659-662. https://doi.org/10.1007/s11431-010-4265-0

Becker KM, 1963. Measurements of convective heat transfer from a horizontal cylinder rotating in a tank of water. *International Journal of Heat and Mass Transfer*, 6(12): 1053-1062. https://doi.org/10.1016/0017-9310(63)90006-1

Chang WR, Etsion I, Bogy DB, 1987. An elastic-plastic model for the contact of rough surfaces. *Journal of Tribology*, 109(2):257-263. https://doi.org/10.1115/1.3261348

Etsion I, 2004. Improving tribological performance of mechanical components by laser surface texturing. *Tribology Letters*, 17(4):733-737. https://doi.org/10.1007/s11249-004-8081-1

Etsion I, 2005. State of the art in laser surface texturing. *Journal of Tribology*, 127(1):248-253. https://doi.org/10.1007/ 978-3-642-03653-8_252

Etsion I, Burstein L, 1996. A model for mechanical seals with regular micro-surface structure. *Tribology Transactions*, 39(3):677-683.

https://doi.org/10.1080/10402009608983582

Etsion I, Kligerman Y, Halperin G, 1999. Analytical and experimental investigation of laser-textured mechanical seal faces. *Tribology Transactions*, 42(3):511-516. https://doi.org/10.1080/10402009908982248

Gropper D, Wang L, Harvey TJ, 2016. Hydrodynamic lubrication of textured surfaces: a review of modeling techniques and key findings. *Tribology International*, 94: 509-529. https://doi.org/10.1016/j.triboint.2015.10.009

Luan Z, Khonsari MM, 2009. A thermohydrodynamic analysis of a lubrication film between rough seal faces. *Proceedings of the Institution of Mechanical Engineers, Part J: Journal of Engineering Tribology*, 223(4):665-673. https://doi.org/10.1243/ 13506501JET456

Meng XK, Bai SX, Peng XD, 2014a. An efficient adaptive finite element method algorithm with mass conservation for analysis of liquid face seals. *Journal of Zhejiang University-SCIENCE A (Applied Physics & Engineering)*, 15(3):172-184. https://doi.org/10.1631/jzus.A1300328

Meng XK, Bai SX, Peng XD, 2014b. Lubrication film flow control by oriented dimples for liquid lubricated mechanical seals. *Tribology International*, 77:132-141. https://doi.org/10.1016/j.triboint.2014.04.020

Meng XK, Zhao WJ, Shen MX, et al., 2018. Thermohydrodynamic analysis on herringbone-grooved mechanical face seals with a quasi-3D model. *Proceedings of the Institution of Mechanical Engineers, Part J: Journal of Engineering Tribology*, 232(11):1402-1414. https://doi:10.1177/1350650117752952

Patir N, Cheng HS, 1978. An average flow model for determining effects of three-dimensional roughness on partial hydrodynamic lubrication. *Journal of Lubrication Technology*, 100(1):12-17. https://doi.org/10.1115/1.3453103

Patir N, Cheng HS, 1979. Application of average flow model to lubrication between rough sliding surfaces. *Journal of Lubrication Technology*, 101(2):220-229. https://doi.org/10.1115/1.3453329

Payvar P, Salant RF, 1992. A computational method for cavitation in a wavy mechanical seal. *Journal of Tribology*, 114(1):199-204. https://doi.org/10.1115/1.2920861

Qiu Y, Khonsari MM, 2011. Performance analysis of full-film textured surfaces with consideration of roughness effects. *Journal of Tribology*, 133(2):021704. https://doi.org/10.1115/1.4003303

Qiu Y, Khonsari MM, 2012. Thermohydrodynamic analysis of spiral groove mechanical face seal for liquid applications. *Journal of Tribology*, 134(2):021703. https://doi.org/10.1115/1.4006063

Shen C, Khonsari MM, 2016. Texture shape optimization for seal-like parallel surfaces: theory and experiment. *Tribology Transactions*, 59(4):698-706. https://doi.org/10.1080/10402004.2015.1110220

Wu C, Zheng L, 1989. An average Reynolds equation for partial film lubrication with a contact factor. *Journal of Tribology*, 111(1):188-191. https://doi.org/10.1115/1.3261872

Xie Y, Li YJ, Suo SF, et al., 2013. A mass-conservative average flow model based on finite element method for complex textured surfaces. *Science China Physics, Mechanics and Astronomy*, 56(10):1909-1919. https://doi.org/10.1007/s11433-013-5217-z

Yang X, Meng XK, Peng XD, et al., 2018. A TEHD lubrication analysis of surface textured mechanical seals. *Tribology*, 38:204-212 (in Chinese). https://doi.org/10.16078/j.tribology.2018.02.011

Yu HW, Wang XL, Zhou F, 2010. Geometric shape effects of surface texture on the generation of hydrodynamic pressure between conformal contacting surfaces. *Tribology Letters*, 37(2):123-130. https://doi.org/10.1007/s11249-009-9497-4

Yu XQ, He S, Cai RL, 2002. Frictional characteristics of mechanical seals with a laser-textured seal face. *Journal of Materials Processing Technology*, 129(1-3):463-466. https://doi:10.1016/S0924-0136(02)00611-8

Zhang H, Hua M, Dong GN, et al., 2016. A mixed lubrication model for studying tribological behaviors of surface texturing. *Tribology International*, 93:583-592. https://doi.org/10.1016/j.triboint.2015.03.027

Zouzoulas V, Papadopoulos CI, 2017. 3-D thermohydrodynamic analysis of textured, grooved, pocketed and hydrophobic pivoted-pad thrust bearings. *Tribology International*, 110:426-440. https://doi:10.1016/j.triboint.2016.10.001

中文概要

题　目： 三角形织构化机械密封的热弹流分析

目　的： 为了提高机械密封的摩擦学特性和密封性能，建立三维热弹性流体动力润滑理论模型来研究三角形织构对机械密封性能的影响，并针对航空轴向柱塞泵机械密封的实际工况，对织构的形状、排布和深度进行优化。

创新点： 1. 建立机械密封热弹性流体动力润滑模型，揭示三角形织构在混合和全膜润滑条件下的减磨减漏机理。2. 以低摩擦和低泄露为目标，采用数值模拟和实验方法，优化三角形织构的形状和排布方式。

方　法： 1. 通过理论推导，建立机械密封热弹性流体动力润滑模型，并与热流体动力润滑模型和流体动力润滑模型进行对比，发现热弹性流体动力模型更

符合实际情况（图 6~10）；2. 通过数值模拟，优化三角形织构的形状、排布以及深度（图 14~22）。3. 通过实验研究，测得织构端面温度，验证热弹流理论模型的正确性（图 25）。

结　论： 1. 由于机械密封的热力变形，密封端面形成收敛性间隙，因此更有利于减少泄漏；2. 与同向排布相比，相向排布的三角形织构能产生更强的流体动压效应，且内外径织构数目越多、数目差距越小时，动压效应越强；3. 直角三角形织构的动压效应强于等边三角形织构，并且在一定工况下能产生足够的液膜承载力使密封端面开启。

关键词： 热弹性流体；机械密封；表面织构；三角形微孔；航空柱塞泵